Performance Evaluation of Silicon-Based Irradiance Sensors Versus Thermopile Pyranometer

Karki, Sameep; Ziar, Hesan; Korevaar, Marc; Bergmans, Thijs; Mes, Joop; Isabella, Olindo

DOI
10.1109/JPHOTOV.2020.3038342

Publication date
2021

Document Version
Final published version

Published in
IEEE Journal of Photovoltaics

Performance Evaluation of Silicon-Based Irradiance Sensors Versus Thermopile Pyranometer

Sameep Karki, Hesan Ziar, Marc Korevaar, Thijs Bergmans, Joop Mes, and Olindo Isabella

***Abstract*—There are several sensors available in the market to measure the plane-of-array irradiance for photovoltaic applications. The prices of these sensors vary according to the design, calibration procedure, and conducted characterization. In this article, two types of silicon-based sensors with and without temperature correction capabilities are compared with a high-accuracy thermopile pyranometer to check their performance. The obtained results showed that silicon-based sensors deviate from the output of the pyranometers. The tested silicon-based pyranometers overestimate the irradiance with the median bias deviations of around 1.43% (with the average measured irradiance of 256 W/m^2). For temperature-corrected silicon pyranometer, the bias deviation is 0.07% with the deviation range of −6.5%–10% (with the average measured irradiance of 257 W/m^2). A working-class reference cell was also tested, resulting in a bias deviation of −1.74% and the deviation range of −13%–7% (with the average measured irradiance of 304 W/m^2). The effect of air mass on the performance of cost-effective sensors was additionally analyzed. Within the measurement time window, the result also showed that for the silicon-based sensors under tests, the effects of the environmental conditions have the following qualitative order of influence: angle of incidence > red-shift > temperature. The performance of silicon-based sensors also showed seasonal dependence, being more accurate during summertime and wintertime, respectively, for the silicon pyranometer and the working-class reference cell. Finally, using the statistical evaluation, simple linear correction functions are introduced for silicon-based sensors.**

***Index Terms*—Air mass (AM), comparison, photovoltaic (PV) module, plane-of-array, reference cell, silicon pyranometer, thermopile pyranometer.**

I. Introduction

THE huge amount of investments in the research and development of photovoltaic (PV) technology has led to the technology becoming affordable and economically viable. The reduction of a PV module price to 0.3 €/Wp has given more incentive all over the world to push forward the sustainable technologies [1]. In spite of this advancement, various factors, such as soiling [2], shading [3], air mass (AM) [4], and temperature [5], considerably influence the performance ratio of PV systems.

An exhaustive study of the PV system performance is needed to know the amount of losses and attain the maximum conceivable electrical yield. This is possible with the help of irradiance sensors available in the market. An irradiance sensor is an instrument that measures the solar power incident per unit area, normally expressed as W/m^2. The instrument is vital to know the total solar power incident at a certain location, analyze the PV system performance, and investigate various loss mechanisms. Irradiance sensors are lightweight, flexible, can be deployed at any condition, and require low power to operate. They are classified into various classes based on their calibration accuracy. The well-known categories of irradiance sensors are thermopile pyranometers, silicon photodiode pyranometers, and PV reference cells.

Thermopile pyranometers measure the total irradiance incident on a flat surface. Using a dome with a 180° field of view, this technology can measure the irradiance from all the directions. The thermal gradient is measured across an area between a hot and cold point. The temperature difference between the hot and cold points is proportional to irradiance. Such devices measure irradiance with a spectral response from 280 to 2800 nm [6].

Silicon photodiode pyranometers consist of a silicon semiconductor embedded behind a diffuser. The photocurrent produced by this semiconductor is proportional to the amount of received irradiance. Such a device can only measure the narrow wavelength range of 300–1100 nm [6].

PV reference cells resemble the properties of a PV module. The photons incident on the PV reference cell generate a current, which can be interpreted as an indicator of irradiance. The reference cell angular response, construction, and materials used can be the same as the target PV module to help for more accurate yield prediction. PV reference cells are classified by following the standard calibration procedure. Primary reference cells are calibrated following the IEC 60904-2 and ASTM 1362-15 standards with the assistance of a pyrheliometer (absolute cavity radiometer in the outdoor environment) [7], [8]. Secondary reference cells are calibrated referring to a primary cell in a solar simulator, while working-class reference cells, the cheaper classified sensors, are calibrated with the help of a secondary reference cell.

The price of irradiance sensors differs based on their calibration procedure. Nowadays, thermopile pyranometers are normally more expensive than silicon pyranometers.

Manuscript received September 30, 2020; revised October 29, 2020; accepted November 7, 2020. Date of publication November 30, 2020; date of current version December 21, 2020. *(Corresponding author: Hesan Ziar.)*

Sameep Karki is with the Delft University of Technology, 2628 CD Delft, The Netherlands (e-mail: sameepkarki0@gmail.com).

Hesan Ziar and Olindo Isabella are with the Photovoltaic Materials and Devices Group, Delft University of Technology, 2628 CD Delft, The Netherlands (e-mail: h.ziar@tudelft.nl; o.isabella@tudelft.nl).

Marc Korevaar, Thijs Bergmans, and Joop Mes are with Kipp & Zonen BV, 2628 XH Delft, The Netherlands (e-mail: marc.korevaar@otthydromet.com; tijs.bergmans@otthydromet.com; joop.mes@otthydromet.com).

Color versions of one or more of the figures in this article are available at https://doi.org/10.1109/JPHOTOV.2020.3038342.

Digital Object Identifier 10.1109/JPHOTOV.2020.3038342

Knowing the importance of irradiance accuracy for PV system calculations, researchers have in the past two decades been examining the performance of various irradiance sensor technologies using real measurements. In [9] and [10], King *et al*. considered PV and photodiode-based irradiance sensors as low-cost devices that can reach a limit of 3% accuracy by using a correction function. The used empirical functions to model the effect of temperature, AM, and angle of incidence (AOI) together with a calibration factor to obtain the desired accuracy range. Although they were successful with obtaining and applying the function but its complexity and need for various inputs could be a potential issue for implementation. Furthermore, Schulz *et al*. [11] compared different types of irradiance sensors considering a few PV module technologies as the reference. They showed that PV reference cells have a lower deviation compared with a thermopile pyranometer and silicon pyranometer. In [12], a project to characterize commercial irradiance sensors, Driesse *et al.* concluded that the sensitivity of irradiance sensors (no matter the technology) to test condition (instrument temperature or AOI) influences the readings error in systematic ways. They also showed that readings of PV reference cells can deviate because of the mismatch in their response spectra. In [13], tests were conducted in two different locations in Germany and the result showed that the reference cell was underperforming when compared with the thermopile pyranometer. In [14], de Montgareuil *et al*. compared silicon photodiode pyranometers and reference cells at varying AM and reported better performance for silicon pyranometers. To increase accuracy, they suggested using the irradiance sensors of the same technology as the cells of the target PV system. Another research showed the deviation of $\pm 10\%$ for both silicon pyranometers and reference cells with respect to the thermopile pyranometers [15]. They reported that PV reference cells performed better during clear sky conditions but deviated more during cloudy days compared with silicon photodiode pyranometers. Finally, a very recent research work [16] assessed the accuracy of low-cost solar irradiance measurement tools installed in 30 personal weather stations. The authors further developed a calibration model based on the temperature of the sensor, solar zenith angle, and clear-sky index that increases the accuracy with the mean bias deviation reduced from $\sim$18% to $\sim$3% for clear sky.

Almost all the literature in this area made an emphasis on the importance of gathering more data and running more tests at different locations. This was the first motivation for this work, and then to look into possible sources of deviation between irradiance sensors, and, finally, to develop simple data-driven correction functions that require a minimum number of inputs for silicon-based sensors to increase their accuracy. Thus, in this article, three silicon pyranometers and a working-class reference cell are compared experimentally with CMP21 thermopile pyranometers from Kipp & Zonen BV. The variations between these sensors are then evaluated.

II. Methodology, Data Collection, and Processing

Three silicon pyranometers ($SP1^{TC}$, SP2, and SP3) and one commercially available working-class reference cell (WRC^{TC}) are installed (TC stands for temperature-corrected). The irradiance data of these silicon-based sensors are compared with the data of a thermopile pyranometer installed right next to the silicon-based sensors. All sensors are in the same plane of array (see Fig. 1). The uncertainty and temperature responses (coefficients) of the sensors are given in Table I. It is worth noting that normally the actual uncertainty values are open to interpretation because of the assumptions and/or methods used to obtain them. The measurement uncertainty, however, depends heavily on local conditions, instrument maintenance, etc. There are several ways how this is calculated by research groups, companies, etc., [18], [19]. For temperature response, there are multiple ways of reporting them, either with a coefficient or with a bandwidth over a temperature range.

The irradiance data were collected from June 26, 2018 to March 31, 2019 using a data logger (CR1000X by Campbell Scientific) [20] and aggregated in a 1-min resolution. Several morning data points were removed because they had huge fluctuations because of shadings (cause by trees, chimneys, and side buildings at the measurement site). The outliers (almost 10% of the data) were removed by comparing the readings from the

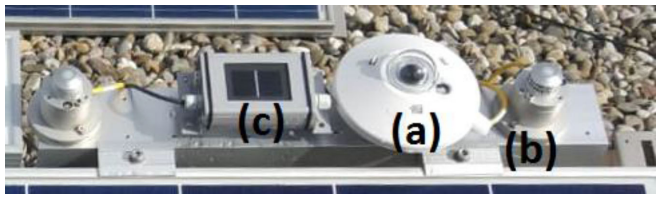

Fig. 1. Part of the measurement setup and different types of irradiance sensors (a) thermopile pyranometer, (b) silicon diode pyranometer, and (c) working-class PV reference cell, which all were tested at the measurement location (Delft, The Netherlands). All the instruments were installed at one mounting structure with a 30° tilt angle facing south (182°). One of the silicon photodiode pyrometers ($SP1^{TC}$) and the working-class reference cell (WRC^{TC}) were temperature corrected. The sensors were cleaned during the monitoring months, quite frequently in the beginning (every few days) and less at the end (every few weeks). The thermopile pyranometer and $SP1^{TC}$ were calibrated, respectively, on Nov. 23, 2017 and May 23, 2018, while both SP1 and SP2 were calibrated on Feb. 7, 2018. The exact calibration date of the WRC^{TC} is unknown to the authors.

TABLE I
Uncertainty and Temperature Responses of the Sensors

Sensor	Calibration uncertainty	Measurement uncertainty (U95)	Temperature response
Thermopile pyr.	1%	4% *	±1% **
$SP1^{TC}$	4%	7% *	±1% **
SP2	4%	7% *	-0.2%/°C #
SP3	4%	7% *	-0.2%/°C #
WRC^{TC}	0.75%	2.5%	±3% ***

Values are obtained or calculated using manufacturers' data, experts' comments, and standard recommendation [17].

#Reported negative temperature response for SP2 and SP3 could be a result of the temperature response of other parts of the device (such as sensing circuitry) impacting the theoretical positive temperature response of the active silicon and turn the overall temperature response negative.

*Depends on measurement conditions.

**Over temperature range of −20–+50 °C.

***Over temperature range of −35–+80 °C.

TABLE II
STATISTICAL DEVIATIONS FOR VARIOUS SENSORS

Sensors	Overall RMSD W/m^2 (%)	Overall MAD W/m^2 (%)	Average sensor W/m^2	Average pyranometer W/m^2 *	Overall Range %	Overall Bias %	Summer Bias %	Winter Bias %
SP1^{TC}	8.34 (3.3)	5.79 (2.3)	257	253	(-6.5, 10)	+0.07	+0.42	-0.72
SP2	9.42 (3.8)	7.21 (2.9)	250	245	(-6.2, 10)	+1.27	+1.47	+1.79
SP3	10.63 (4.1)	8.06 (3.1)	262	261	(-7.5, 12)	+1.59	+1.93	+1.93
WRC^{TC}	13.83 (4.4)	9.36 (3.0)	304	312	(-13, 7)	-1.74	-2.01	-0.96

Percentage values are normalized values with respect to the average thermopile pyranometer measurements.
*Since outliers happened at different times for different silicon sensors, the corresponding average pyranometer recordings differ per silicon-based sensor.

thermopile pyranometer and the target silicon sensor. The upper and lower bands for data filtering were obtained using $UB = Q3 + 1.5 \times IQR$ and $LB = Q1 - 1.5 \times IQR$, where Q3 and Q1 are the third and first quartile, respectively and IQR is the interquartile range.

In addition, to know the effect of AM on the performance accuracy of the sensors, at each time instant, the AM was calculated by [21], [22]

$$\mathrm{AM} = \frac{\exp(-z/z_h)}{\sin a_s + 0.50572(a_s + 6.07995)^{-1.6364}} \quad (1)$$

where z is the site altitude (10 m), z_h is the scale height of the Rayleigh atmosphere near the earth's surface, which is 8434.5 m, and a_s is the sun altitude.

Differences between the reference (CMP21 thermopile pyranometer) and tested instruments were considered as "deviations" while acknowledging that the CMP21 might also have sources of error. If the median of the data distribution is not equal to the pyranometer value, there is a bias in the test instruments. Besides the bias deviation, a further assessment was carried out using statistical indicators, such as mean absolute deviation (MAD) and root mean square deviation (RMSD). The equations for the statistical indicators can be found in [23]. Additionally, the boxplot diagrams that give an inclusive view of deviation distributions are used to represent the deviation quantiles. The data sets were further divided into subjects for the winter and summer weather to determine the seasonal performance of the instruments.

III. RESULTS AND DISCUSSION

This section presents the results of outdoor measurements. First, the variation between the overall data is discussed. Then, the data are evaluated separately for the summer and winter months. Next, the effect of AM on the deviation of silicon-based sensors with respect to the thermopile pyranometer is investigated. Finally, the correction factors are introduced.

A. Overall Performance of the Silicon-Based Sensors

Fig. 2(a) shows the deviation distribution of datasets for the sensors mentioned in Section II. The deviations of SP2 and SP3 sensors range from -18 to 30 W/m^2. Both SP2 and SP3 overestimate the irradiance with a median deviation bias of almost 4 W/m^2, whereas for SP1^{TC}, the bias deviation is approximately 0.17 W/m^2, which is significantly lower. The deviation range for SP1^{TC} is -17 to 26.5 W/m^2. The WRC^{TC} underestimates the irradiance with the deviation ranging from -39 to 22.4 W/m^2 and a bias of -5.43 W/m^2 (the highest bias deviation and deviation range among the sensors). Alongside the respective boxplot, the red and the blue bars show the RMSD as a merit for precision and MAD as the merit for accuracy. Thermopile pyranometers are slow compared with silicon sensors. However, the response time of tested sensors is way less than 1 min and the reported recordings are average values over every minute, which reduces the effects of the temporal variations of the sensors on the reported deviations. Data outliers were also removed prior to statistical analysis. The statistical indicators have been summarized in Table II.

The overall performance of different irradiance sensors with respect to the thermopile pyranometer shows that the WRC^{TC} sensor has a low calibration accuracy and, thus, considered to be a working-class reference cell. The silicon pyranometers SP2 and SP3 have a bias compared with the CMP21 pyranometer and, therefore, lack somewhat in the accuracy of the calibration. The bias and, therefore, the assumed calibration of SP1^{TC}, however, is close to the thermopile pyranometer. It is worth noting that the calibration accuracy is not the only factor affecting the observed bias deviation because the bias value reduces in winter months yet always exists and is the same for SP2 and SP3 sensors. Therefore, it is fair to say that the observed bias deviation and the calibration accuracy are related.

B. Seasonal Performance

Here, the performance of irradiance sensors are assessed during summer months with high sun elevation, more sun hours, and mostly clear days, and during winter months with low sun elevation, fewer sun hours, and fluctuating weather conditions (sunny, cloudy, and even snowy days). The snow, fog, and water droplets also cause high data variation between two seasonal sets of data. The winter months have fewer data points (33% less) because of fewer sun hours.

Fig. 2(b) and (c) shows an absolute deviation distribution of tested sensors during summer and winter. Table II lists the relative seasonal deviations. From Table II, it can be seen that the working-class reference cell is more accurate during winter (with almost the same precision as summer), whereas silicon pyranometers perform better during summer with higher accuracy and precision. This behavior can be explained by the fact that WRC is very sensitive to the AOI, while in winter (because

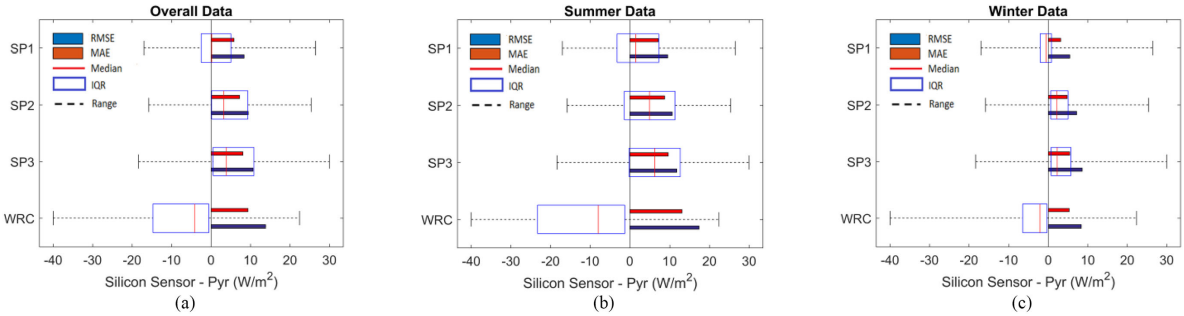

Fig. 2. Error distribution of cost-effective sensors when compared with the thermopile pyranometer. The acronyms $SP1^{TC}$, SP2, and SP3 are for three silicon pyranometers, respectively, while WRC^{TC} is for the working-class reference cell. (a) Overall, (b) summer months from Jun. 26, 2018 to Sep. 30, 2018, and (c) winter months from Oct. 1, 2018 to Feb. 28, 2019. The boxplots demonstrate the interquartile range (blue box), the median (red line), and the extended range of the data distribution without outliers.

of cloudiness) the AOI effect decreases and helps the sensor to perform better. On the other hand, as in winter, the spectral red-shift is more than in summer, then silicon pyranometers (that have diffusers and are less sensitive to AOI) act more accurately in summer.

C. Air Mass Effect

In this section, the silicon-based irradiance sensors are compared with the thermopile pyranometer considering AM. The path length for sunlight to travel through the atmosphere increases with increasing AM. Changing AM shows its effect in three ways. By increasing the AM (e.g., sun going down in the horizon), the spectrum makes a red-shift, the AOI increases, and the temperature drops. In theory, increasing the temperature, AOI, and red-shift should, respectively, increase, decrease, and increase the output of a silicon-based sensor. Having this in mind, it is interesting to observe the influence of these changes on the plots in Fig. 3, which shows the ratio of the reference pyranometer values with respect to the silicon-based sensors (Pyr/silicon-based sensor) versus the AM value over a day. A clear day (July 3, 2018) was selected for this analysis. For $SP1^{TC}$, only red-shift (see Fig. 4) is supposed to make influence because the device is both temperature and cosine corrected (cosine correction refers to the technical approaches used in irradiance sensors to suppress or eliminate the effect of AOI). However, the slight deviations during high AM suggest that possibly the cosine correction of the device is not perfect for AOI values more than 60°, or the reference point for the temperature correction is set higher than the instrument temperature. For SP2 and SP3, since they are cosine corrected, the temperature and red-shift are expected to make an influence. The overall outputs of SP2 and SP3 increase as AM increases (and within a wide range of AM their output is almost constant), whereas the temperature reduction (or even AOI increase) should have in theory decreased the output. However, according to Table I, SP2 and SP3 have negative temperature coefficients, which together with the red-shift cause such behavior. For WRC^{TC}, AOI plays the dominant role and severely affects the device output. Having these plots, it can be concluded that for the tested silicon-based

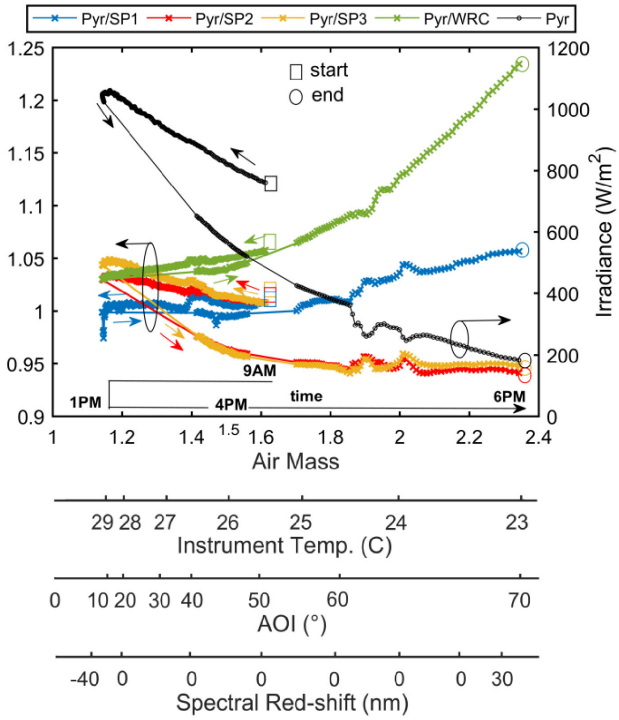

Fig. 3. Effect of AM on the ratio between the output of pyranometer and silicon-based sensors (July 3, 2018 from 9 A.M. to 6 P.M.). The variation of instrument temperature (measured for the thermopile pyranometer while all irradiance sensors had a similar body temperature), AOI (calculated using the sun's position and instrument orientation), and spectral shift (calculated using local ambient conditions and SMARTS 2.9.5 [24]) are also shown in the figure. It can be seen that from A.M. 1.2 to 2.2 the peak on which the maximum irradiance happens shifts slightly (red-shift). The fluctuations in the graphs are beause of shading from side objects and passing clouds. The communication failure caused a few data gaps but the trend is recognizable by the lines between the markers. The starting and ending points are shown for each set of data, respectively, using squares and circles. In addition, the arrows are added to show the trends of the data over the course of the day. As the response curve of silicon sensors increases from 400 to 1000 nm (despite the constant response of thermopile pyranometer over a wide range of spectrum), red-shift causes the output of silicon sensors to increase [25]–[27]. Multiple data points at the same AM values are because of the similarity of AM during a few hours in the morning and afternoon. The ambient temperature was between 20 and 25 °C during measurements. Except WRC^{TC}, all sensors have diffusers for cosine correction, while only WRC^{TC} and $SP1^{TC}$ have temperature correction. Note that the plots show the values of thermopile pyranometer/silicon sensors, therefore, the values above unity mean the underestimation and vice versa.

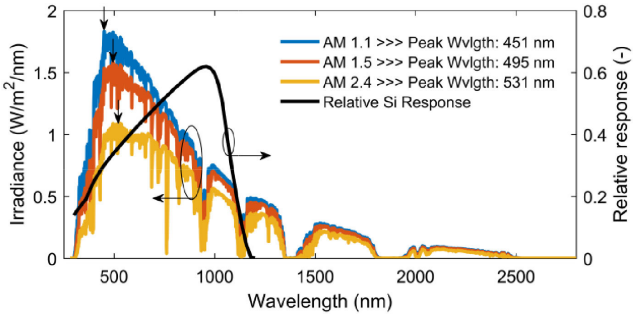

Fig. 4. SMARTS generated spectra with the spectral response of a typical silicon-based sensor, which is the spectral response of the HOQ mono-cSi reference cell reported by Fraunhofer ISE [28]. The spectra are global tilted irradiance aligned with sensors installation plane and have been generated for the location condition of Delft, The Netherlands, considering the weather condition July 3, 2018. The peaks for each sky spectrum are shown with arrows, showing the red-shift. The spectrum red-shift results in an increase in the response of a silicon-based sensor as long as the shift is small enough to fit in the device response window, which is the case for this study.

TABLE III
STATISTICAL DEVIATIONS BEFORE AND AFTER CALIBRATION

Sensors	Before calibration		After calibration	
	RMSE W/m² (%)	MAE W/m² (%)	RMSE W/m² (%)	MAE W/m² (%)
$SP1^{TC}$	8.34 (3.3)	5.79 (2.3)	8.32 (3.3)	5.80 (2.3)
SP2	9.42 (3.8)	7.21 (2.9)	8.26 (3.4)	6.16 (2.5)
SP3	10.63 (4.1)	8.06 (3.1)	9.33 (3.6)	6.96 (2.7)
WRC^{TC}	13.83 (4.4)	9.36 (3.0)	7.85 (2.5)	5.31 (1.7)

sensors, the effects of the environmental condition within the measurement time window has the following qualitative order of importance: *AOI* > *red-shift* > *temperature.*

Overall, $SP1^{TC}$ agrees with the thermopile pyranometer during low AM and slightly underestimates during high AM. SP2 and SP3 showed less deviation than other sensors during high AM. The WRC^{TC} highly underestimates the irradiance during high AM conditions. The high dependence of WRC^{TC} on AM suggests less installation of them in higher latitudes (for irradiance sensing per se).

D. Correction Functions

Having a database of measured values and considering a thermopile pyranometer as the reference, empirical correction functions were obtained to correct the response of the silicon-based sensors. The obtained empirical correction functions have the general form of $c_1 \cdot R + c_2$, where R is the sensor readings. The values of c_1 and c_2 for each sensor are obtained by linear fitting, as shown in Fig. 5. To assess the effect of correction functions on the accuracy (MAD) and precision (RMSD) of the silicon-based sensors, a comparison is made before and after applying the correction functions. As can be seen in Table III, the correction coefficients are most effective on the tested working-class reference cell. The added value of empirical correction functions is that the silicon-based sensors (especially working-class reference cells) can also have reasonable accuracy. Despite its simplicity, a *possible* disadvantage of this method could be its location- and case-dependence. For future research, after collecting and analyzing the considerable amount of data from different types of irradiance sensors installed at various locations, it is recommended that the solar resource sector of the PV community implement artificial intelligence approaches to improve the accuracy of the silicon-based sensors, which can bring a financial benefit.

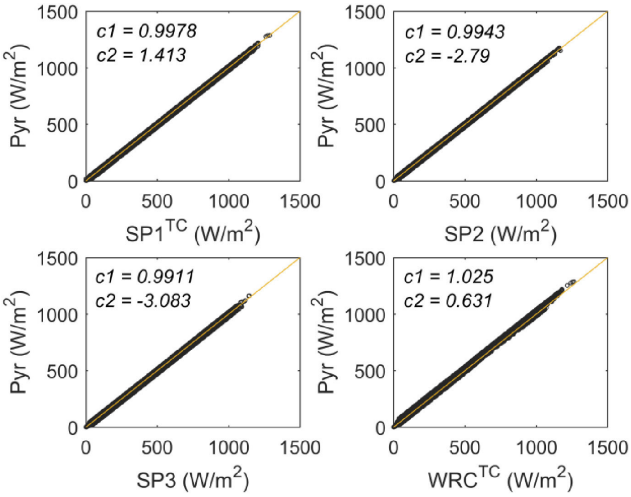

Fig. 5. Linear fits of thermopile pyranometer versus silicon-based sensors. The calibration excellency of the device is shown for each plot. Corrections factors were obtained based on 1-min data for nine months and can be further improved using a more enriched dataset. The correction values are only applicable in Delft, The Netherlands, and might change with the location because of different environmental conditions.

IV. CONCLUSION

The data collected from different silicon-based sensors were compared with the thermopile pyranometer data (for a period of nine months with a 1-min resolution). Although a limited number of sensors were studied in this work and more data from different locations are advisable, valuable results were obtained. The silicon-based pyranometers and working-class reference cell output had a high range of deviation when compared with a thermopile pyranometer. The tested silicon-based pyranometers underestimated the irradiance with the median bias deviations of around 1.43%. However, using the temperature correction shifted the bias deviation to 0.07%. The tested working-class reference cell resulted in a bias deviation of -1.74%. In the winter months, the WRC works more accurately, while the silicon pyranometers are more accurate and precise during summertime. Qualitatively speaking, the silicon-based sensors have the highest sensitivity first to AOI, then to the sunlight spectrum, and, finally, to temperature variations. The silicon-based sensors can be calibrated with simple data-driven empirical corrections with respect to a high-accuracy thermopile pyranometer. The tested working-class reference cell benefited the most from the correction function, showing RMSD and MAD drop from 4.4% to 2.5% and 3% to 1.7%, respectively. Extending the presented study by gathering data from more number of sensors installed at various places can lead to more conclusive results.

ACKNOWLEDGMENT

Results presented in this work is for one specific location, The results might differ based on locations and environmental conditions.

REFERENCES

[1] "Photovoltaics report," Fraunhofer Inst. Sol. Energy Syst., Freiburg, Germany, 2019.

[2] P. Nepal, M. Korevaar, H. Ziar, O. Isabella, and M. Zeman, "Accurate soiling ratio determination with incident angle modifier for PV modules," *IEEE J. Photovolt.*, vol. 9, no. 1, pp. 295–301, Jan. 2019.

[3] H. Ziar *et al.*, "Quantification of shading tolerability for photovoltaic modules," *IEEE J. Photovolt.*, vol. 7, no. 5, pp. 1390–1399, Sep. 2017.

[4] Y. Nakada, H. Takahashi, K. Ichida, T. Minemoto, and H. Takakura, "Influence of clearness index and air mass on sunlight and outdoor performance of photovoltaic modules," *Curr. Appl. Phys.*, vol. 10, no. 2, pp. S261–S264, 2010.

[5] J. Kurnik, M. Jankovec, K. Brecl, and M. Topic, "Outdoor testing of PV module temperature and performance under different mounting and operational conditions," *Sol. Energy Mater. Sol. Cells*, vol. 95, no. 1, pp. 373–376, 2011.

[6] R. Rösemann and C. Lee, "A guide to solar radiation measurement: From sensor to application: An overview of the state of the art: UV, visible," Kipp & Zonen, 2011.

[7] *Photovoltaic Devices - Part 3: Measurement Principles for Terrestrial Photovoltaic (PV) Solar Devices With Reference Spectral Irradiance Data*, Int. Org. Standardization, Geneva, Switzerland, IEC Standard 60904-3, 2008.

[8] *Standard Test Methods for Calibration of Non-Concentrator Photovoltaic Non-Primary Reference Cells*, ASTM Int., West Conshohocken, PA, USA, ASTM Standard E1362-15, 2019.

[9] D. L. King, W. E. Boyson, W. I. Bower, and B. R. Hansen, "Improved accuracy for low-cost solar irradiance sensors," in *Proc. 2nd World Conf. Exhib. Photovolt. Sol. Energy Convers.*, Vienna, Austria, 1998, pp. 1–4.

[10] D. L. King and D. R. Myers, "Silicon-photodiode pyranometers: Operational characteristics, historical experiences, and new calibration procedures," in *Proc. Conf. Rec. 26th IEEE Photovolt. Specialists Conf.*, 1997, pp. 1285–1288.

[11] B. Schulz *et al.*, "Evaluation of calibrated solar cells and pyranometers regarding the effective irradiance detected by PV modules," in *Proc. 25th Eur. Photovolt. Sol. Energy Conf. Exhib.*, 2012, pp. 4797–4800.

[12] A. Driesse, W. Zaaiman, D. S. Riley, N. Taylor, and J. S. Stein, "Indoor and outdoor evaluation of global irradiance sensors," in *Proc. 31st Eur. Photovolt. Sol. Energy Conf.*, Hamburg, Germany, 2015, pp. 14–18.

[13] M. Zehner *et al.*, "One year round robin testing of irradiation sensors—Measurement results and analyses," in *Proc. 24th Eur. Photovolt. Sol. Energy Conf.*, 2009, pp. 3800–3805.

[14] A. G. de Montgareuil, J.-L. Martin, F. Mezzasalma, and J. Merten, "Main results of the first intercomparison campaign of European irradiance sensors at Ines Cadarache," in *Proc. 22nd Eur. Photovolt. Sol. Energy Conf.*, Milan, Italy, 2007, pp. 14–18.

[15] F. Vignola *et al.*, "Comparison of pyranometers and reference cells on fixed and one-axis tracking surfaces," in *Proc. Amer. Sol. Energy Soc. Sol. Conf.*, 2017, pp. 1–10.

[16] J. L. Lorente, X. Liu, and D. J. Morrow, "Worldwide evaluation and correction of irradiance measurements from personal weather stations under all-sky conditions," *Sol. Energy*, vol. 207, pp. 925–936, 2020.

[17] ISO/IEC GUIDE 98-3:2008, "Uncertainty of measurement—Part 3: Guide to the expression of uncertainty in measurement," 1993, pp. 1–120.

[18] W. Bich, M. G. Cox, and P. M. Harris, "Evolution of the 'Guide to the expression of uncertainty in measurement'," *Metrologia*, vol. 43, no. 4, pp. 161–166, 2006.

[19] A. Habte, M. Sengupta, I. Reda, A. Andreas, and J. Konings, "Calibration and measurement uncertainty estimation of radiometric data," in *Proc. Sol.*, San Francisco, CA USA, 2014, pp. 1–7.

[20] "CR1000 measurement and control datalogger," Campbell Sci., Inc., Logan, UT, USA, 2020. [Online]. Available: https://www.campbellsci.com/cr1000

[21] C. Rigollier, O. Bauer, and L. Wald, "On the clear sky model of the ESRA—European solar radiation atlas—With respect to the Heliosat method," *Sol. Energy*, vol. 68, no. 1, pp. 33–48, 2000.

[22] F. Kasten and A. T. Young, "Revised optical air mass tables and approximation formula," *Appl. Opt.*, vol. 28, no. 22, pp. 4735–4738, 1989.

[23] Z. Jin, W. Yezheng, and Y. Gang, "General formula for estimation of monthly average daily global solar radiation in China," *Energy Convers. Manage.*, vol. 46, no. 2, pp. 257–268, 2005.

[24] C. A. Gueymard, "SMARTS Code, version 2.9. 5 User's manual," Sol. Consulting Services, 2005. [Online]. Available: http://www.solarconsultingservices. com/SMARTS295_manual.pdf

[25] H. Ziar, F. F. Sönmez, O. Isabella, and M. Zeman, "A comprehensive albedo model for solar energy applications: Geometric spectral albedo," *Appl. Energy*, vol. 255, no. , 2019, Art. no. 113867.

[26] H. Liu *et al.*, "The impact of haze on performance ratio and short-circuit current of PV systems in Singapore," *IEEE J. Photovolt.*, vol. 4, no. 6, pp. 1585–1592, Nov. 2014.

[27] *Solar Energy—Specification and Classification of Instruments for Measuring Hemispherical Solar and Direct Solar Radiation*, ISO Standard 9060, 1990.

[28] Flyer: Reference cells, "Fraunhofer Institute for Solar Energy Systems ISE," pp. 1–2. [Online]. Available: https://www.ise.fraunhofer.de/content/dam/ise/de/documents/infomaterial/brochures/photovoltaik/17_en_ISE_Flyer_ReferenceCells.pdf